Biophysical Journal, Volume 98

Supporting Material

Exploring the conformational space of chromatin fibers and their stability by numerical dynamic phase diagrams

René Stehr, Robert Schöpflin, Ramona Ettig, Nick Kepper, Karsten Rippe, and Gero Wedemann

SUPPLEMENTARY MATERIALS

Exploring the conformational space of chromatin fibers and their stability by numerical dynamic phase diagrams

René Stehr[*], Robert Schöpflin[*], Ramona Ettig[†], Nick Kepper[†], Karsten Rippe[†], Gero Wedemann[*1]

[*] University of Applied Sciences Stralsund, System Engineering and Information Management, Zur Schwedenschanze 15, 18435 Stralsund, Germany

[†] Deutsches Krebsforschungszentrum & BIOQUANT, Research Group Genome Organization & Function, Im Neuenheimer Feld 280, 69120 Heidelberg, Germany

[1] to whom correspondence should be addressed: gero.wedemann@fh-stralsund.de

SUPPLEMENTARY METHODS

Representation of the chromatin chain in the six-angle model

As described in (1), the chromatin fiber is defined by a linear chain of segments, one for each nucleosome and two or three segments describing the intervening linker DNA. The position of the segment *i* in the chain is described by a position vector $\vec{p}_i$, while its orientation is described by a local coordinate system ($\vec{f}_i, \vec{u}_i, \vec{v}_i$) with $\vec{v}_i = \vec{u}_i \times \vec{f}_i$. The segment vector $\vec{s}_i$ is defined by $\vec{s}_i = \vec{p}_{i+1} - \vec{p}_i$ with the segment length $b_i = |\vec{s}_i|$ and $\vec{s}_i = \vec{u}_i \cdot b_i$. The geometrical center $\vec{m}_i$ of the nucleosome *i* is given by:

$$\vec{m}_i = \vec{p}_i + \frac{1}{2}\vec{s}_i + c \cdot \hat{a}_i, \qquad \text{(SM1)}$$

where *c* is the distance between the center of the segment and the nucleosome center, and $\hat{a}_i$ is the vector describing the direction from the segment center to the nucleosome center (Fig. SM1).

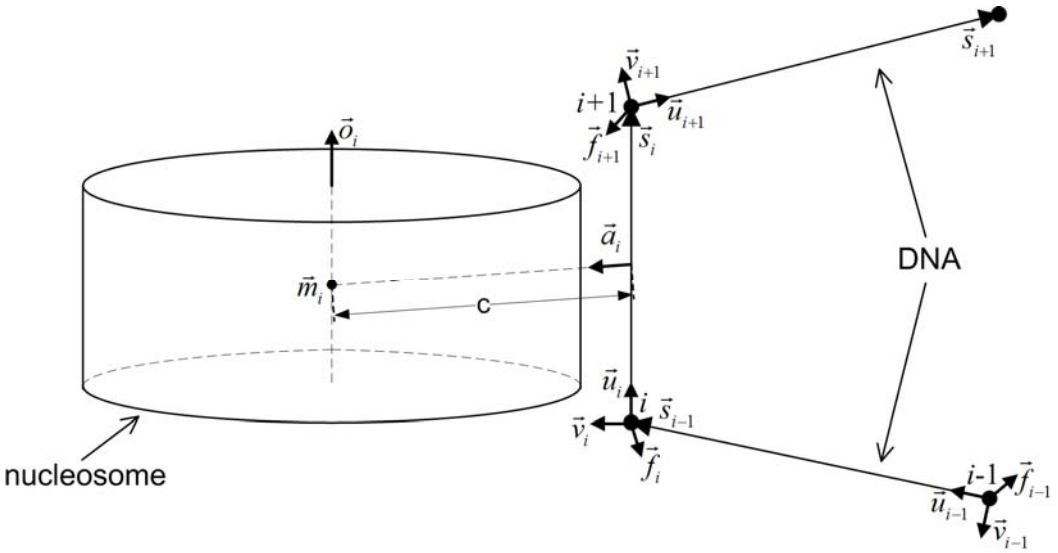

FIGURE SM1. Discretization of the chromatin fiber. Three segments are shown: *i* is the segment of the nucleosome, and *i*-1 and *i*+1 are segments of the incoming and outgoing linker DNA. For simplification, the shape of the nucleosome is shown as cylinder instead of a spherocylinder as it is used for the calculation of the internucleosomal interaction energy (see below).

In the previously used two-angle representation, for $\vec{a}_i$ and $\vec{o}_i$ holds: $\vec{a}_i = \vec{v}_i$ and $\vec{o}_i = \vec{u}_i$ (1). Thus, the orientation of the nucleosome was parallel to the segment vector and the center was situated symmetrically with respect to the segment vector. In contrast, in the six-angle model the nucleosome center and orientation can be shifted and rotated relative to the segment vector (2). Therefore, $\vec{a}_i$ is defined by two rotations of the vector $\vec{v}_i$: around $\vec{u}_i$ by the angle ε and around $\vec{f}_i$ by the angle ϕ (2) (Figs. 1 *A* and SM1). Similarly, $\vec{o}_i$ is described by two rotations of the vector $\vec{u}_i$: around $\vec{v}_i$ by the angle δ and around $\vec{f}_i$ by the angle ζ (Figs. 1 *A* and SM1). Note that ζ is not included in former descriptions of the six-angle model, since it has not been needed for the description of fiber conformations studied. The nucleosome description of the six-angle model (2) is compatible with the description of the two-angle model (1) if the angles ε, ϕ, δ and ζ are set to 0°. For more details see Fig. 1 *A* and the corresponding text.

Elastic energies

The elastic interactions described in (1) are assumed to be harmonic. The strength constants of the interactions are named $a_{(Y)}^{(X)}$ in which X denotes the type of interaction. This can be stretching (s), bending (b) or torsion (t). The interaction partners are denoted by Y, which can be either DNA or nucleosome. The stretching energy is defined by:

$$U_{Stretch} = \frac{a_Y^{(s)}}{b_i^0}\left(b_i - b_i^0\right)^2, \qquad \text{(SM2)}$$

with b_i is the current length of the segment as described above and b_i^0 is the equilibrium length of the segment. The equilibrium length is defined by the chosen DNA linker length divided by the number of segments between adjacent nucleosomes. For nucleosomes, b_i^0 is defined as the equilibrium distance *d* between incoming and outgoing DNA (Fig. 1 *A*).

For the bending energy, an equilibrium nucleosome geometry is defined by the incoming and outgoing linker DNA. The bending angle is computed between the segment vector $\vec{u}_{i+1}$ and its equilibrium direction $\vec{B}_i$ relative to the connected segment. $\vec{B}_i$ is defined by the angles ω_i and ξ_i:

$$\vec{B}_i = \vec{f}_i \sin\omega_i \cos\xi_i + \vec{v}_i \sin\omega_i \sin\xi_i + \vec{u}_i \cos\omega_i \qquad \text{(SM3)}$$

and the bending angle θ_i is calculated from $\cos(\theta_i) = \vec{B}_i \vec{u}_{i+1}$. The bending energy is given by:

$$U_{Bend} = \frac{a_Y^{(b)}}{b_i^0}\theta_i^2 \qquad \text{(SM4)}$$

The angles ω_i and ξ_i for the intrinsic bending of two segments i and i+1 are defined by the parameters α and γ of the six-angle model (Fig. 1 *A*):

$$\xi_i = \begin{cases} (\pi-\alpha)/2 & ,if\ i \in NUC \wedge i+1 \in DNA \\ \pi/2 & ,if\ i \in DNA \wedge i+1 \in NUC \\ 0 & ,if\ i \in DNA \wedge i+1 \in DNA \end{cases} \qquad \text{(SM5)}$$

$$\omega_i = \begin{cases} (-\pi+\gamma)/2 & ,if\ i \in NUC \wedge i+1 \in DNA \\ (-\pi+\gamma)/2 & ,if\ i \in DNA \wedge i+1 \in NUC \\ 0 & ,if\ i \in DNA \wedge i+1 \in DNA \end{cases} \qquad \text{(SM6)}$$

In the two-angle model (1), the equilibrium entry-exit angle of the DNA at the nucleosome was defined by α measured parallel to the flat side of the nucleosome cylinder. In the six-angle model, the additional angle γ describes the entry-exit-angle measured perpendicular to the flat side of the nucleosome cylinder (Fig. 1 *A*). If γ = 0°, the equilibrium position of the six-angle model (Eqs. SM5 and SM6) corresponds to the two-angle model.

For the torsion energy, an intrinsic torsion is considered. The coordinate systems of two connected segments i and i+1 can be mapped on each other by an Euler-transformation with the angles (α_i, β_i, γ_i) in which the rotation of the first angle is around $\vec{u}_i$. Then $\alpha_i + \gamma_i - \tau_i$ is the total torsion with τ_i is the intrinsic torsion. The torsion potential is then:

$$U_{Torsion} = \frac{a_Y^{(t)}}{b_i^0}\left(\alpha_i + \gamma_i - \tau_i\right)^2 \qquad \text{(SM7)}$$

The intrinsic torsion τ_i of two segments i and i+1 is defined by the parameters α and β of the two- and six-angle model (Fig. 1 *A*):

$$\tau_i = \begin{cases} \beta - \pi - \alpha/2 & ,if\ i \in NUC \wedge i+1 \in DNA \\ -\alpha/2 & ,if\ i \in DNA \wedge i+1 \in NUC \\ 0 & ,if\ i \in DNA \wedge i+1 \in DNA \end{cases} \qquad \text{(SM8)}$$

Electrostatic Energy

The electrostatic interaction between DNA segments is determined by integrating the solution of the Debye-Hückel equation for a point charge over two charged line segments (1):

$$E_{ij}^{(e)} = \frac{\nu^2}{D} \int d\lambda_i \int d\lambda_j \frac{\exp(-\kappa r_{ij})}{r_{ij}} \qquad \text{(SM9)}$$

D is the dielectric constant of water, and κ the inverse of the Debye length. r_{ij} is the distance between the current positions at the segments i and j to which the integration parameters λ_i, λ_j correspond. The charge per unit length ν is chosen such that the potential at the radius of the DNA coincides with the solution of the Poisson-Boltzmann equation for a cylinder with charge per length ν_0^*. For DNA in the presence of the Gouy layer of immobile counterions, this can be computed as $\nu_0^* = q\nu_0$ in which $\nu_0 = -2e/\Delta$ is the charge per length of the naked DNA (3), e is the proton charge, and Δ = 0.34 nm is the distance between base pairs. Following Stigter, the value of q is 0.73 (4). To save computation time, a tabulation of the double integral is used. The table is parameterized by the distance of the segments and three values describing its relative orientation. During the simulation a linear interpolation of the tabulated values was used.

Internucleosomal potential

The anisotropic internucleosomal interaction is described by a series expansion in S-functions (5). This potential is based on the 12-6 Lennard-Jones potential:

$$U(\hat{o}_1,\hat{o}_2,\vec{r}) = 4\varepsilon(\hat{o}_1,\hat{o}_2,\hat{r})\left[\left(\frac{\sigma_0}{|\vec{r}|-\sigma(\hat{o}_1,\hat{o}_2,\hat{r})+\sigma_0}\right)^{12}-\left(\frac{\sigma_0}{|\vec{r}|-\sigma(\hat{o}_1,\hat{o}_2,\hat{r})+\sigma_0}\right)^{6}\right], \quad \text{(SM10)}$$

with $\hat{o}_1$ and $\hat{o}_2$ as unit vectors defining the orientation of the particles (see above), $\vec{r}$ as the vector of the distance of the particles ($\vec{r} = \vec{m}_2 - \vec{m}_1$) and σ_0 scales the potential width. The potential strength (ε) and range (σ) parameters depend on the orientation and center-to-center difference vectors of two nucleosomes and define the anisotropy of the potential. For the Zewdie potential, the two factors were described by S-functions for identical cylindrically symmetric particles (6, 7). The potential range is defined as:

$$\sigma(\hat{o}_1,\hat{o},\hat{r}) = \sigma_0[\sigma_{000}S_{000} + \sigma_{cc2}(S_{202}+S_{022}) + \sigma_{220}S_{220} + \sigma_{222}S_{222} + \sigma_{224}S_{224}], \quad \text{(SM11)}$$

and the potential strength is given by:

$$\varepsilon(\hat{o}_1,\hat{o}_2,\hat{r}) = \varepsilon_0[\varepsilon_{000}S_{000} + \varepsilon_{cc2}(S_{202}+S_{022}) + \varepsilon_{220}S_{220} + \varepsilon_{222}S_{222} + \varepsilon_{224}S_{224}], \quad \text{(SM12)}$$

where ε_0 is the maximum potential strength. The S-functions (S_{000}, S_{202}, S_{022}, S_{220}, S_{222} and S_{224}) depend on the orientation of the nucleosomes and the difference vector between the nucleosome centers. They are listed in Table SM1. The expansion coefficients for the strength (ε_{000}, ε_{cc2}, ε_{220}, ε_{222}, ε_{224}) and range (σ_{000}, σ_{cc2}, σ_{220}, σ_{222}, σ_{224}) are responsible for the dimension of the nucleosome shape and for the ratio of the energy strength between different oriented nucleosomes (e.g., top-on-top and side-by-side), respectively. While the range coefficients were chosen in order to fit the dimensions of the nucleosome (width = 11 nm and height = 5.5 nm), the strength expansion coefficients were chosen to achieve a ratio of 1/12 between side-by-side and top-on-top oriented nucleosomes (5). The actual values for these coefficients as well as for the range parameter were determined by performing least square fits (5) and are shown in Table SM2.

TABLE SM1. The first six S-functions for identical cylindrically symmetric particles. $\hat{o}_1$ and $\hat{o}_2$ are the unit vectors defining the orientation of the particles (Fig. SM1) and $\hat{r}$ is the unit vector of the center-to-center distance of the particles.

$f_0 = \hat{o}_1 \cdot \hat{o}_2$, $f_1 = \hat{o}_1 \cdot \hat{r}$, $f_2 = \hat{o}_2 \cdot \hat{r}$.
$S_{000} = 1$, $S_{202} = (3f_1^{\,2} - 1)/2\sqrt{5}$, $S_{022} = (3f_2^{\,2} - 1)/2\sqrt{5}$, $S_{220} = (3f_0^{\,2} - 1)/2\sqrt{5}$,
$S_{222} = (2 - 3f_1^2 - 3f_2^2 - 3f_0^2 + 9f_1 f_2 f_0)/\sqrt{70}$,
$S_{224} = (1 + 2f_0^2 - 5f_1^2 - 5f_2^2 - 20f_0 f_1 f_2 + 35f_1^2 f_2^2)/4\sqrt{70}$

TABLE SM2. Parameters of the nucleosome-nucleosome potential for the ratio $E_{lateral}/E_{longitudinal}$ = 1/12 between the maximum interaction energy of lateral and longitudinal oriented nucleosomes.

Parameter	**Value**
S000	1.6957
Scc2	-0.7641
S220	-0.1480
S222	-0.2582
S224	0.5112
E000	2.7206
Ecc2	6.0995
E220	3.3826
E222	7.1036
E224	3.2870
σ_0	5.5 nm

In order to demonstrate the anisotropy of this potential, Fig. SM2 shows the energy of two nucleosomes in dependence of their distance and orientation for ε_0 = 0.5 k_BT (k_B is the Boltzmann constant and T is the temperature). It is apparent that for the top-on-top arrangement the highest attraction energy $E_{\max}$ appears, which corresponds to $12 \cdot \varepsilon_0$ (14.6 kJ/mol), while the side-by-side arranged nucleosomes lead to a maximum attraction energy of ε_0 (1.2 kJ/mol).

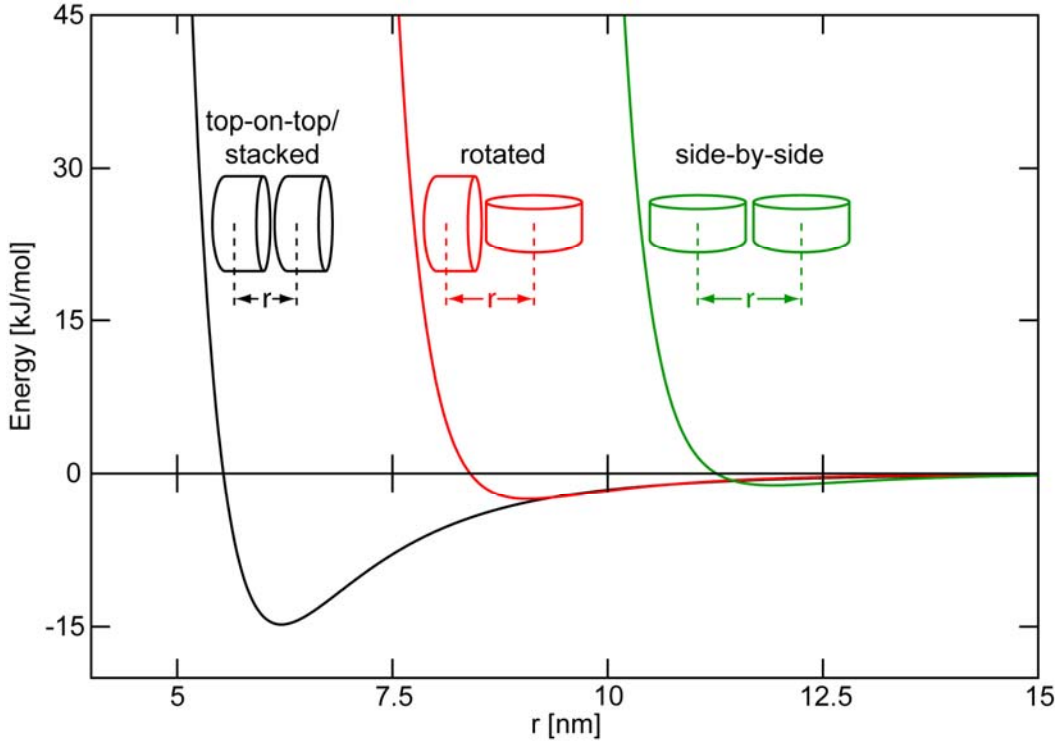

FIGURE SM2. Zewdie-Potential as function of the center-to-center distances r for different oriented nucleosome pairs. The parameters of the potential are shown in Table SM2. The maximum potential depth of top-on-top and side-by-side arranged nucleosomes deviates by the factor 12. For all curves, the energy is zero at the distance where nucleosomes touch each other: $r_{top\text{-}on\text{-}top}$ = 5.5 nm, $r_{rotated}$ = 8.25 nm and $r_{side\text{-}by\text{-}side}$ = 11 nm.

DNA-Nucleosome excluded volume

In order to inhibit sterical overlaps between nucleosomes and linker DNA, a repulsive potential is defined. Therefore, the DNA is approximated by a number of overlapping spheres with the radius r_d = 1.2 nm corresponding to the DNA cylinder radius. Similar to the Zewdie potential, the nucleosome is represented as a spherocylinder with the particular condition that the radius and height are defined by r_n = 5.5 nm, which correspond to the nucleosome dimension (width = 11 nm and height = 5.5 nm) (Fig. SM3 *A*). The repulsion energy between a DNA linker and a nucleosome with the segment indices *D* and *N*, respectively, is defined by the summation of the interaction energy of each DNA-sphere with the nucleosome:

$$E_{DNA-Nuc} = \sum_{i=1}^{S} E'_{DNA-Nuc}\left(\vec{m}_N, \vec{o}_N, \vec{e}_{D,i}\right), \qquad \text{(SM 13)}$$

where S is the number of spheres per DNA segment, $\vec{m}_N$ and $\vec{o}_N$ are the center and orientation vectors of the nucleosome N (Fig. SM1), respectively, and $\vec{e}_{D,i}$ is the center of the ith sphere of the DNA segment D:

$$\vec{e}_{D,i} = \vec{p}_D + \vec{s}_D \cdot r_d + (i-1)\frac{b_D - 2r_d}{S-1}\vec{s}_D . \qquad \text{(SM 14)}$$

As described above, $\vec{s}_D$ is the segment D, $\vec{p}_D$ is the starting point of the segment, and b_D is the length of the segment (Fig. SM1). The energy $E'_{DNA-Nuc}$ of one DNA-sphere and a nucleosome is defined by:

$$E'_{DNA-Nuc}(\vec{m},\vec{o},\vec{e}) = \begin{cases} 0, & \text{if } d(\vec{m},\vec{o},\vec{e}) \geq r_n + r_d \\ k \cdot \left(d(\vec{m},\vec{o},\vec{e}) - r_n - r_d\right)^{12}, & else \end{cases} , \qquad \text{(SM 15)}$$

with k is the energy scaling constant. The parameter $d(\vec{m},\vec{o},\vec{e})$ defines the minimum distance between the center of the DNA sphere $\vec{e}$ and the nucleosome center axis, which is defined by the center $\vec{m}$ and the orientation $\vec{o}$ of the nucleosome (Fig. SM1). The distance $d(\vec{m},\vec{o},\vec{e})$ is computed from the projection of the DNA-sphere center on the plane of the nucleosome center axis. Accordingly, the vector $\vec{n}$ defines the projection point of the DNA-sphere center on the plane of the nucleosome center axis (Fig. SM3 *B*):

$$\vec{n} = \vec{e} - \left(\hat{o} \cdot (\vec{e} - \vec{m})\right) \cdot \hat{o} , \qquad \text{(SM 16)}$$

and the vector $\vec{q} = \vec{n} - \vec{m}$ is the distance between this point and the nucleosome center. Thus, the distance $d(\vec{m},\vec{o},\vec{e})$ is calculated by:

$$d(\vec{m},\vec{o},\vec{e}) = \begin{cases} \left|\vec{e} - \vec{n}\right|, & if \ \left|\vec{q}\right| < r_n / 2 \\ \left|\vec{e} - \left(\vec{m} + \frac{r_n}{2} \cdot \hat{q}\right)\right|, & else \end{cases} . \qquad \text{(SM17)}$$

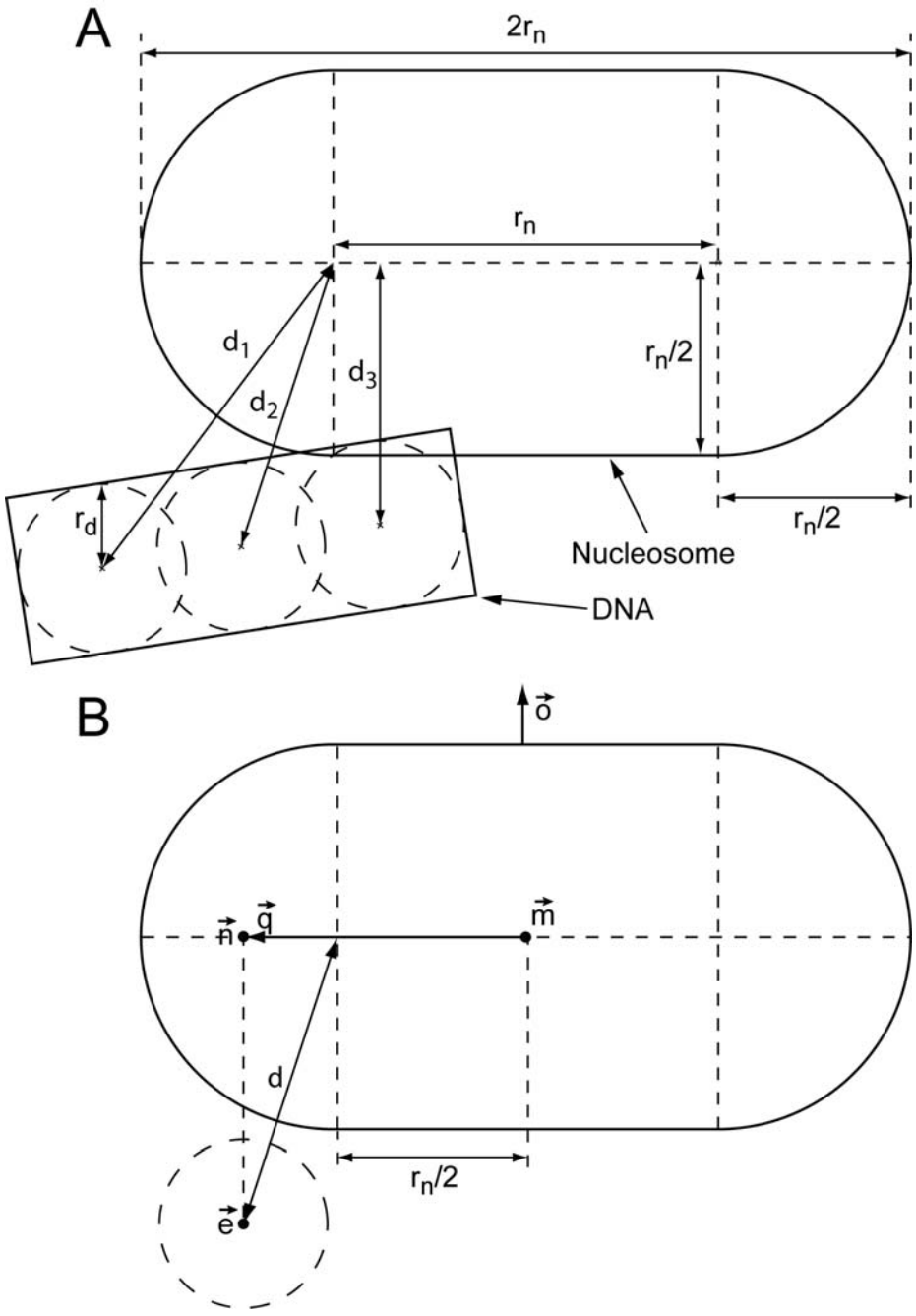

FIGURE SM3. Schematic representation of the DNA-nucleosome excluded volume. (A) The nucleosome is represented as spherocylinder with the radius and height r_n, while the DNA cylinder is approximated by a number of spheres, in this case three, with the radius r_d. The distances d_1, d_2 and d_3 indicate the minimum distances between the nucleosome center axis and the DNA spheres. An overlap occurs if $d < r_d + r_n$. In this example, the third sphere exhibits an overlap since $d_3 < r_d + r_n$. (B) The distance d between a DNA-sphere and the nucleosome is computed by the projection point $\vec{n}$ of the DNA-sphere center $\vec{e}$ on the plane of the nucleosome center axis (Eq. SM16). If the length of the vector $\vec{q}$ is smaller than $r_n/2$, then d is the distance between $\vec{e}$ and $\vec{n}$, otherwise d is defined by the distance between $\vec{e}$ and $\vec{m} + \hat{q} \cdot r_n/2$ (Eq. SM 17).

SUPPLEMENTARY TABLES

TABLE S1. Parameters used in the MC simulations. The elastic parameters were chosen as described by Wedemann and Langowski (1). For the DNA, the values are based on the average of experimentally determined values of 45 - 50 nm DNA bending persistence length and a DNA torsion elasticity of $2.8 \pm 0.2 \cdot 10^{-19}$ J nm (8). The elasticity of the nucleosome/chromatosome has not been derived from experimental studies. Therefore, values were chosen that essentially maintain the initial conformation of the chromatosome.

Parameter	Value
Stretching module DNA	$1.10 \cdot 10^{-18}$ J nm
Bending module DNA	$2.06 \cdot 10^{-19}$ J nm
Torsion module DNA	$2.67 \cdot 10^{-19}$ J nm
Electrostatic radius DNA	1.2 nm
Stretching module nucleosome	$1.10 \cdot 10^{-18}$ J nm
Torsion module nucleosome	$1.30 \cdot 10^{-18}$ J nm
Temperature	293 K
Ionic strength	100 mM NaCl

Table S2. Six-angle model geometries and properties for different chromatin fiber models. The CL and ID structures were developed in (2) and the CLS geometry in (5). The diameter and linear mass density were computed from the statistical ensemble in thermal equilibrium. The ID geometry with NRL > 187 bp did not lead to an obvious nucleosome stacking pattern, and structures with NRL = 207 bp did not form fiber-like structures in thermal equilibrium (2).

Geometry	**NRL** (bp)	ψ (°)	α (°)	γ (°)	β (°)	ε (°)	ϕ (°)	δ (°)	c (nm)	d (nm)	**Fiber Type** [N_{stack}, N_{step}]	**diameter** (nm)	**linear mass density** (nucleosomes/11 nm fiber)
CL	169	70	50	-50	220	0	0	20	3.3	8	[2, 1]	26.2 ± 0.2	3.1 ± 0.1
CLS	212	26	26	0	260	0	0	0	8	3.1	[3, 1]	36 ± 0.7	4.6 ± 0.1
ID	187	128	117.5	-65	0	0	0	60	5.6	3.7	[6, 1]	30.1 ± 0.1	7.6 ± 0.2
ID	197	121	117.5	-39	0	0	0	58	5.6	3.7	—	37.5 ± 0.4	6.9 ± 0.5
ID	207	120	117.5	-28	0	0	0	52	5.6	3.7	—	—	—

TABLE S3. Energies of simulated chromatin structures at different simulation steps. The remaining parameters of the six-angle model correspond to the descriptions of Table S2. For each system, the energy for three stages of the simulations is shown: i) before simulation corresponding to the values of the static phase diagrams (static PD), ii) after 10^7 Monte Carlo (MC) steps corresponding to the dynamic phase diagrams (dynamic PD), and iii) the mean value for the simulated structure in thermal equilibrium. The differences between the energies of simulated structures after 10^7 MC steps (dynamic PD) and the mean values in thermal equilibrium are marginal.

Geometry	**NRL** (bp)	ψ (°)	α (°)	γ (°)	β (°)	**energy static PD** (k_BT)	**energy dynamic PD** (k_BT)	**mean energy thermal equilibrium** (k_BT)
former models (see refs.(2, 5), Fig. S1 and Table S2)								
CL	169	70	50	-50	220	197078	383	426 ± 28
CLS	212	26	26	0	260	106601	369	361 ± 28
ID	187	128	117.5	-65	0	35450	99	98 ± 28
ID	197	121	117.5	-39	0	239	168	138 ± 31
ID	207	120	117.5	-28	0	1114	312	320 ± 32
new models (see Fig. 5 and Table 1)								
CL	169	25	17.7	-17.7	175	201991	208	290 ± 35
ID	187	117.5	117.5	0	295	96882	21	55 ± 28
ID	187	125	117.5	-54.23	355	94898	46	88 ± 28
ID	197	130	117.5	-70.89	355	-75	14	89 ± 27

SUPPLEMENTARY FIGURES

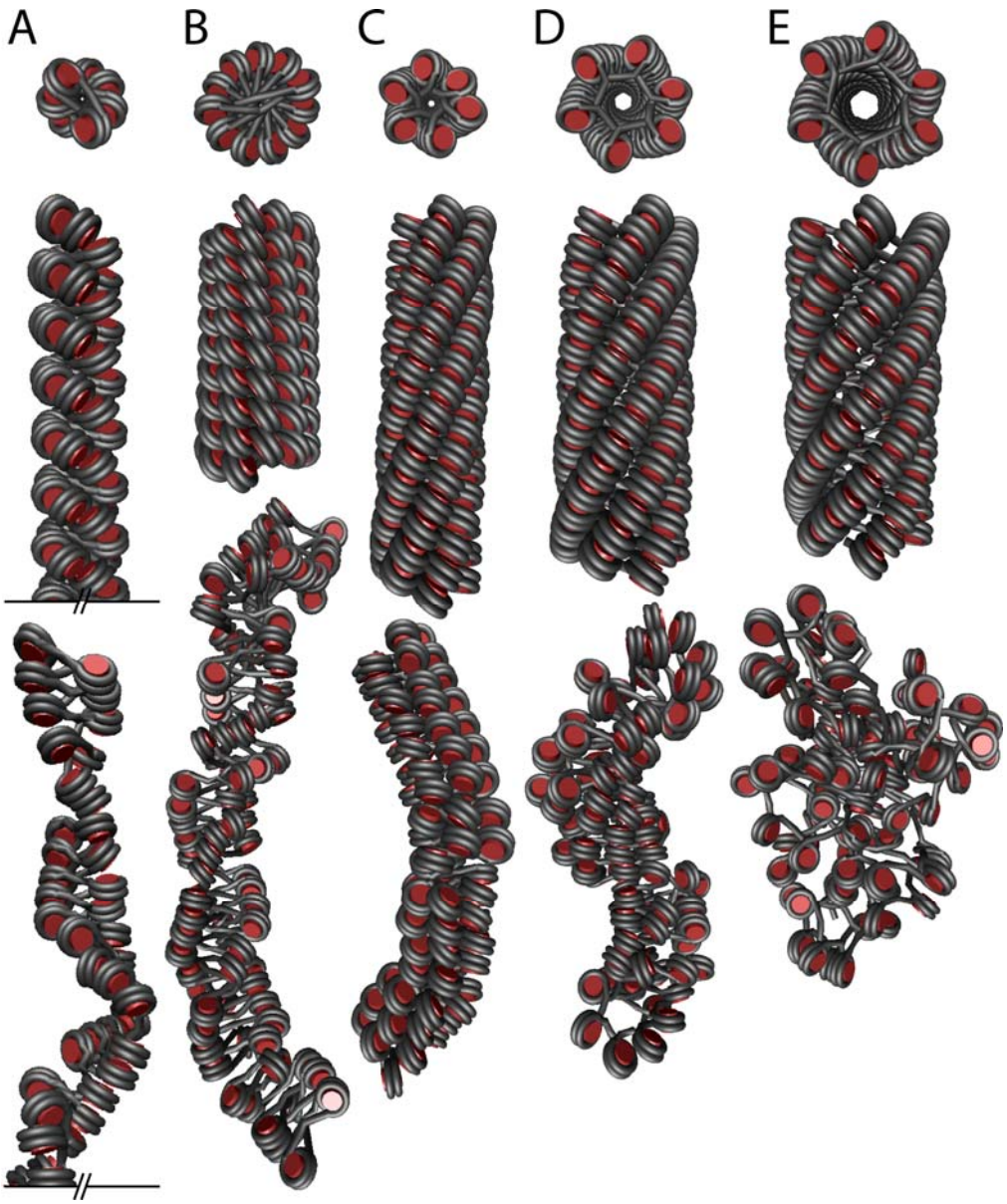

FIGURE S1. Chromatin fiber models for different nucleosome geometries. The configurations were generated by MC simulations. The simulated fibers are designated according to the denotation of Depken and Schiessel (9) (Fig. 1 *B*). (A) Crossed-linker (CL) geometry derived from the tetranucleosome crystal-structure (2) lead to a [2, 1] fiber. (B) Crossed-linker model with nucleosome stem (CLS) for native chromatin of chicken erythrocytes (5) lead to a partially broken [3, 1] fiber. (C, D, E) Interdigitated geometry (ID) including linker histones with NRL of 187, 197 and 207 bp, respectively. These models were developed to reproduce the experimental data of reconstituted chromatin fibers with high mass densities (2). For an NRL of 187 bp, a [6, 1] fiber is obtained (C), while for higher NRLs (D and E) no uniform nucleosome stacking occurred.

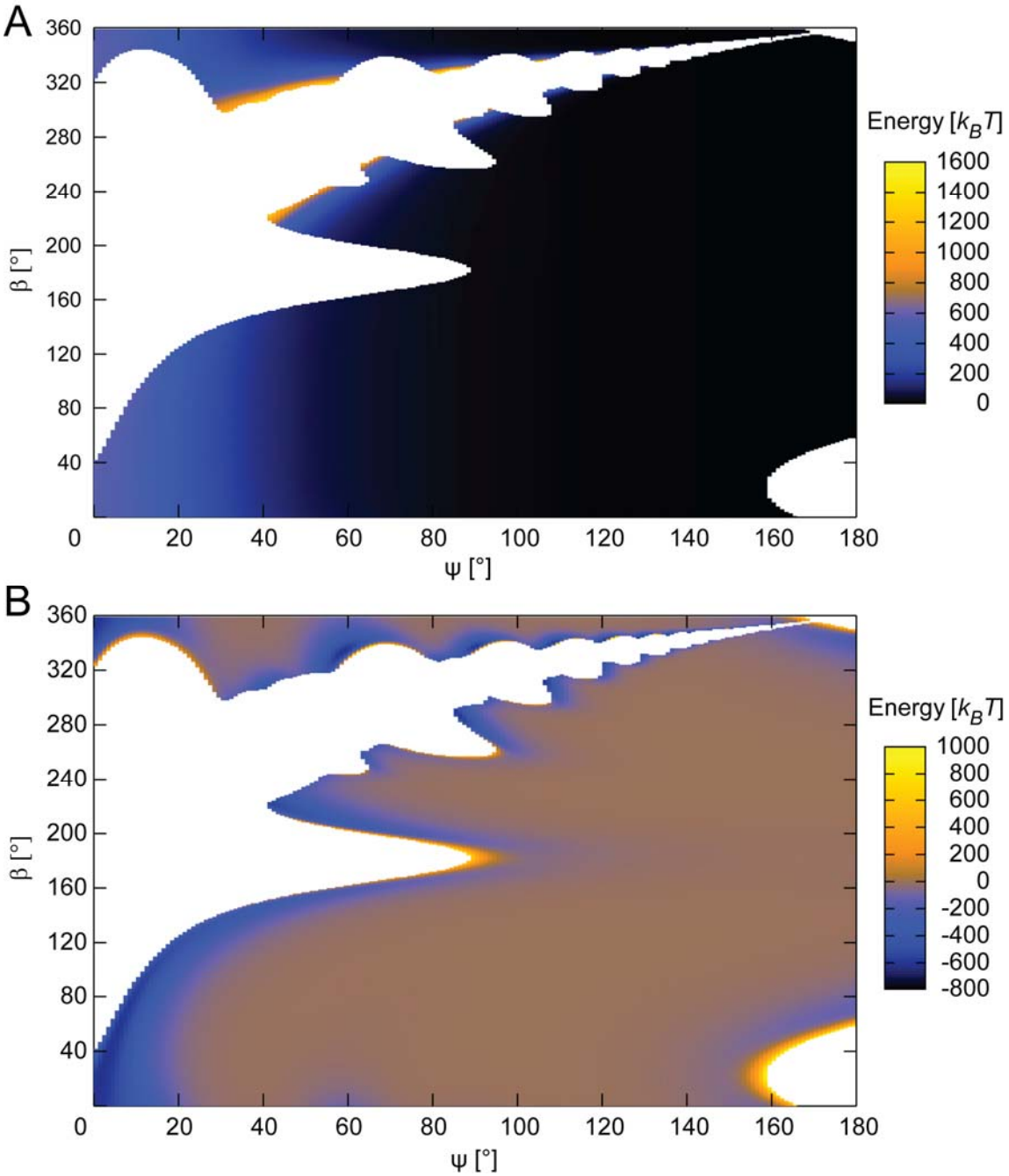

FIGURE S2. Static phase diagrams of single energies of the CLS geometry with NRL = 212 bp for the opening angle ψ ($\gamma = 0$) and the nucleosome twist angle β with a step width of 1°. The corresponding phase diagram of the total energy is shown in Fig. 2 *B*. (A) Electrostatic energy of the linker DNA segments. The highest energies occur at the border between sterically possible and impossible conformations. However, there are also borders with very low electrostatic energy. (B) Energy of the nucleosome-nucleosome interaction. The lowest energy appears near the border between sterically possible and impossible conformations.

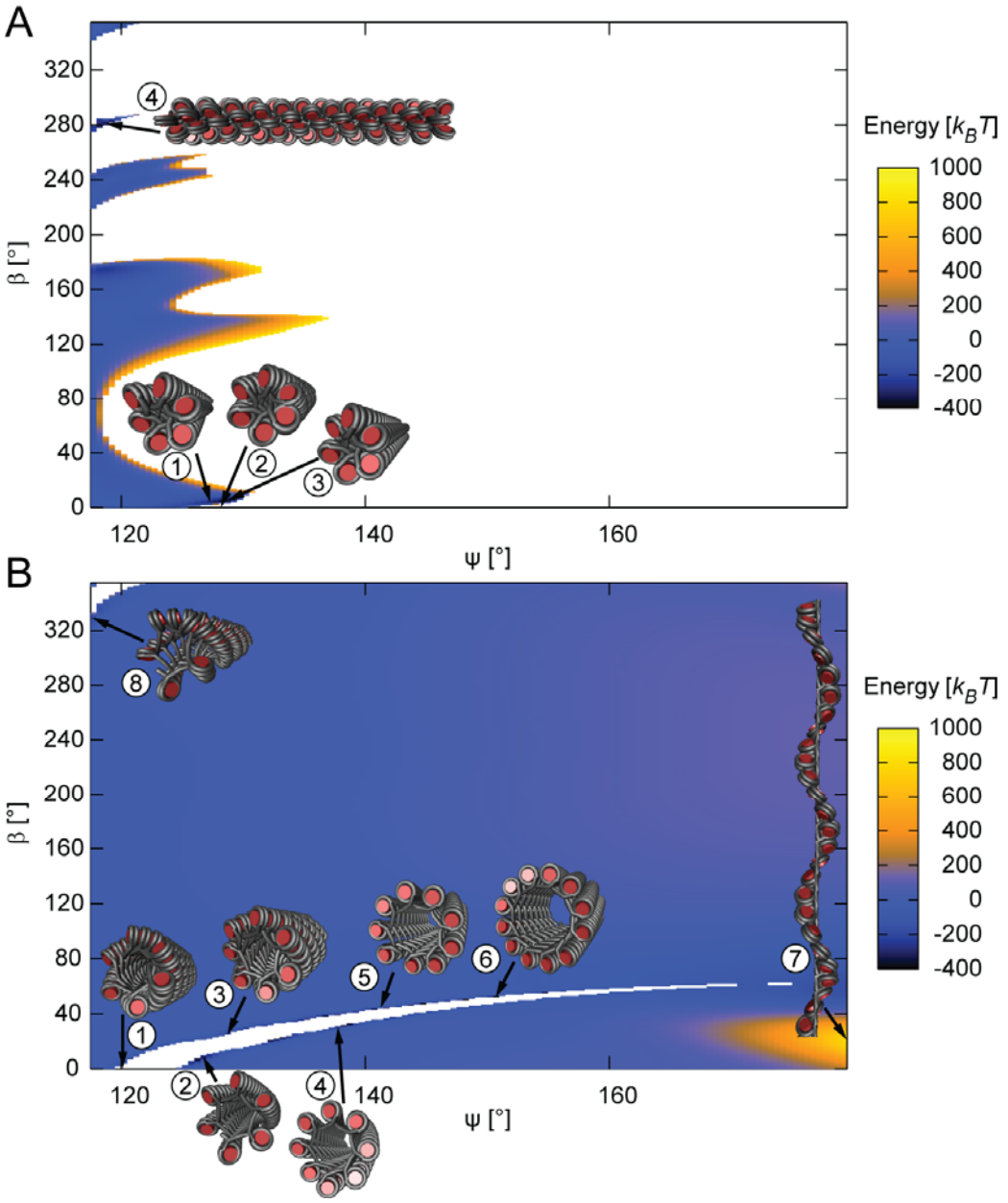

FIGURE S3. Energy phase diagrams for the ID geometry. A value of α = 117.5° was used, while γ was varied in order to reach the indicated value of the opening angle ψ. Step widths of 0.5° and 1° were used for ψ and β, respectively. Fibers with the lowest energy were found at the border between sterically possible and impossible conformations. Previous models for reconstituted chromatin fibers in the elastically relaxed state are located in sterically forbidden areas (A: fiber 2, B: fiber 1). (A) NRL = 187 bp. Broad energy valleys are apparent for two fiber types: [6, 1] fibers with nucleosomes perpendicular to the fiber axis (fibers 1 and 3), and fibers with nucleosomes parallel to the fiber axis with no apparent nucleosome stacking (fiber 4). (B) NRL = 207 bp. No obvious energy valleys exist but fibers with a high number of nucleosome stacks and large diameter had the lowest energies (fibers 2-6 and 8). These interdigitated fibers can be described by [n, 1] where n is the number of nucleosome stacks in the range of 5 (fiber 8), 12 (fiber 6) and above for higher ψ values (fibers not shown).

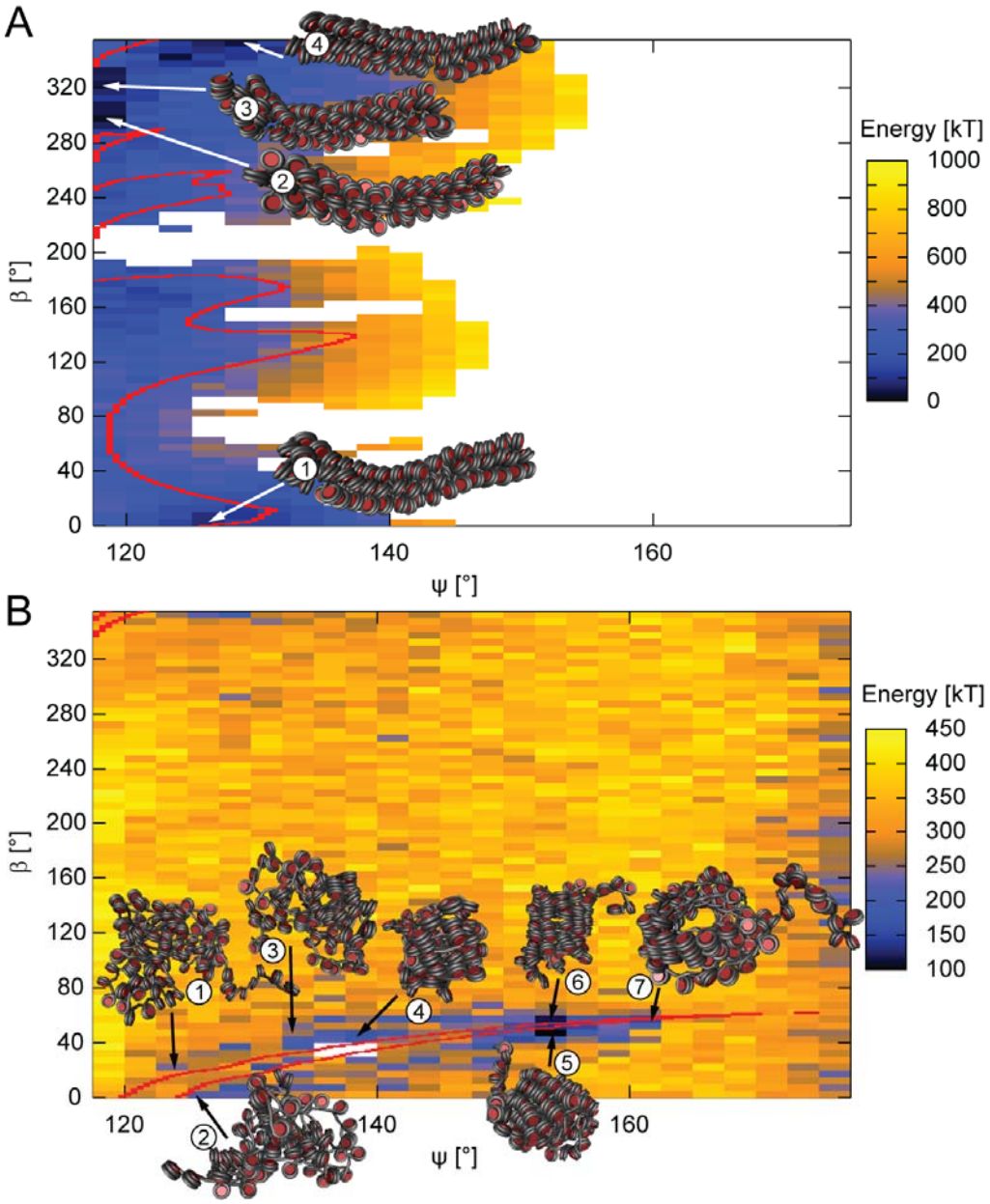

FIGURE S4. Dynamic energy phase diagrams of the ID geometry for the opening angle ψ and the nucleosome twist angle β. Simulations for 10^7 MC steps were conducted and the last configurations of the simulated trajectories were used for analysis. The red contour lines indicate the former borderline between the sterically possible and impossible conformations of the static phase diagrams (Fig. S3). For both NRLs, the chromatin structures became more irregular and the region of the sterically forbidden area reduced significantly. (A) NRL = 187 bp. Two different structures are energetically most favorable: ID fibers with nucleosomes parallel to the fiber axis, e.g., fiber 2 with no apparent nucleosome stacking, and fibers with nucleosomes perpendicular to the fiber axis, e.g., [5, 1] (fiber 3) and [6, 1] (fibers 1 and 4) fiber conformations. (B) NRL = 207 bp. Most of the chromatin fibers did not retain their initial conformation during the simulations (fibers 1-4). Only fibers with a high number of nucleosome stacks (> 11) and high diameters (> 47 nm) converged to stable fiber-like structures, e.g., fiber 5: [12, 1], fiber 6: [13, 1], and fiber 7: [17, 1].

REFERENCES

1. Wedemann, G., and J. Langowski. 2002. Computer simulation of the 30-nanometer chromatin fiber. Biophys J 82:2847-2859.
2. Kepper, N., D. Foethke, R. Stehr, G. Wedemann, and K. Rippe. 2008. Nucleosome geometry and internucleosomal interactions control the chromatin fiber conformation. Biophys J 95:3692-3705.
3. Schellman, J., and D. Stigter. 1977. Electrical double layer, zeta potential, and electrophoretic charge of double stranded DNA. Biopolymers 16:1415–1434.
4. Stigter, D. 1977. Interactions of highly charged colloidal cylinders with applications to double stranded DNA. Biopolymers 16:1435–1448.
5. Stehr, R., N. Kepper, K. Rippe, and G. Wedemann. 2008. The Effect of Internucleosomal Interaction on Folding of the Chromatin Fiber. Biophys J 95:3677-3691.
6. Stone, A. J. 1978. The description of bimolecular potentials, forces and torques: the S and V function expansions. Molec. Phys. 36:241–256.
7. Zewdie, H. 1998. Computer-simulation studies of diskotic liquid crystals. PHYSICAL REVIEW E 57:1793-1805.
8. Bloomfield, V. A., D. M. Crothers, and I. Tinocco. 2000. Nucleic Acids Structures, Properties, and Functions. University Science Books.
9. Depken, M., and H. Schiessel. 2009. Nucleosome shape dictates chromatin-fiber structure. Biophys J 96:777–784.